MATERIALS SCIENCE

Enhanced thermoelectric performance of heavy-fermion compounds YbTM_2Zn$_{20}$ (TM = Co, Rh, Ir) at low temperatures

Kaya Wei[1], Jennifer N. Neu[1,2], You Lai[1,2], Kuan-Wen Chen[1,2], Dean Hobbis[3], George S. Nolas[3], David E. Graf[1], Theo Siegrist[1,4], Ryan E. Baumbach[1,2]*

Thermoelectricity allows direct conversion between heat and electricity, providing alternatives for green energy technologies. Despite these advantages, for most materials the energy conversion efficiency is limited by the tendency for the electrical and thermal conductivity to be proportional to each other and the Seebeck coefficient to be small. Here we report counter examples, where the heavy fermion compounds YbTM_2Zn$_{20}$ (TM = Co, Rh, Ir) exhibit enhanced thermoelectric performance including a large power factor (PF = 74 μW/cm-K^2; TM = Ir) and a high figure of merit (ZT = 0.07; TM = Ir) at 35 K. The combination of the strongly hybridized electronic state originating from the Yb *f*-electrons and the novel structural features (large unit cell and possible soft phonon modes) leads to high power factors and small thermal conductivity values. This demonstrates that with further optimization these systems could provide a platform for the next generation of low temperature thermoelectric materials.

INTRODUCTION

Efficient thermoelectric materials show a confluence between the opposing properties of being poor thermal conductors and good electrical conductors and supporting a large induced voltage in response to a temperature gradient (thermopower) (*1*). While electrical current is only carried by electrons, heat current is carried by both electrons and lattice vibrations (phonons). This necessitates that a useful material will feature mechanisms through which phonons are strongly scattered but electrical conduction remains unperturbed, i.e., the "phonon-glass, electron-crystal" concept (*1*). An effective way to accomplish this has been realized in materials with large cage-like voids in their atomic arrangement that can be filled with loosely bound heavy ions that scatter phonons as they "rattle" (*2*, *3*). To maximize the thermopower, a material must have a large and rapidly changing density of states near the Fermi energy (*4*, *5*). This is accomplished in some *f*-electron materials, where the Kondo effect results in strong hybridization between the narrow *f*-level band and the broad metallic conduction band. In these Kondo lattice systems, it is often seen that there is an anomalously large Seebeck coefficient that peaks in the vicinity of the Kondo coherence temperature, i.e., the temperature range where the emergent heavy Fermi liquid begins to form due to hybridization effects (*6*–*9*). On the basis of such features, strategies that combine soft lattice phonon modes and Kondo lattice effects have previously been pursued in a variety of systems, most notably the filled skutterudites and chemical/structural relatives, but only with limited success (*10*).

Motivated by these earlier studies, we synthesized high-purity single crystals of YbTM_2Zn$_{20}$ (TM = Co, Rh, Ir) to assess their thermoelectric properties. These materials were earlier reported to form in a cubic structure that includes large Zn polyhedrons that coordinate the Yb ions (*11*). Important features of this structure include its large unit cells, a cage-like covalent framework, and low coordination numbers for the constituent atoms, all of which suggest that they could be good candidates for thermoelectric applications (*2*, *3*). The cage dimensions of YbTM $_2$Zn$_{20}$, defined as the longest distance between the two vertices in the cage frame, are around 6 Å, which is comparable to that of many filled skutterudites that show soft lattice phonon modes (*1*, *12*, *13*). Earlier work also shows that these compounds exhibit heavy-fermion behavior that emerges from the Yb Kondo lattice. Evidence for this include (i) that they have large electronic Sommerfeld coefficients due to enhanced mass [also seen in effective mass determined from the de Haas–van Alphen (dHvA) experiment (*14*)] change carrier quasiparticles; (ii) that the Kadowaki-Woods ratio is obeyed, reinforcing the conclusion that the enhanced Sommerfeld coefficient is a property of an enhanced mass Fermi liquid; (iii) that the electrical transport and the magnetic susceptibility exhibit Kondo coherence peaks; and (iv) that tuning of the electronic state using applied pressure produces a phase diagram that conforms to expectations from the Doniach phase diagram (*15*–*20*). As TM evolves from Co→Rh→Ir, the Kondo coherence temperature increases from roughly 1 to 10 K (*15*, *18*–*20*), suggesting that these materials would be expected to exhibit chemically tunable large thermopowers at low temperatures. More generally, other Yb-containing thermoelectric materials also show promising features at high temperatures for power generation applications (e.g., Yb$_{14}$MnSb$_{11}$) (*21*). Despite these attractive features, to our knowledge, there has been no investigation of the thermoelectric figure of merit of the 1-2-20 family of compounds.

Here, we report single-crystal x-ray diffraction (XRD) measurements and the temperature (T) dependence of the thermopower (S), electrical resistivity (ρ), heat capacity (C_p), thermal conductivity (κ), and thermoelectric figure of merit ($ZT = S^2T/\rho\kappa$) for this family of materials. Our XRD measurements reveal atomic displacement parameters to be around 0.01 Å for the Yb ions (Table 1). This value is relatively small, yet in the same order of magnitude, compared with that in other materials with soft lattice modes. The averaging of the anisotropic vibrational modes may play a role here (*22*). We also find that the lattice thermal conductivity (κ_L) is strongly reduced by the soft lattice phonon modes, with values in the range of 2 to 5 W/m-K for all three compounds (minimized for the TM = Ir analog). The low-temperature ρ varies depending on the coherence temperature of the materials but is roughly similar for all three compounds, with values

---

[1] National High Magnetic Field Laboratory, Florida State University, Tallahassee, FL, USA. [2] Department of Physics, Florida State University, Tallahassee, FL, USA. [3] Department of Physics, University of South Florida, Tampa, FL, USA. [4] Department of Chemical and Biomedical Engineering, FAMU-FSU College of Engineering, Tallahassee, FL, USA.
*Corresponding author. Email: baumbach@magnet.fsu.edu

Table 1. Structural diameters from single-crystal XRD and fitting parameters of κ_L using the Debye model as described in the text. The results from fitting C_p based on the combined Debye-Einstein model are in parentheses.

Specimen	$YbCo_2Zn_{20}$	$YbRh_2Zn_{20}$	$YbIr_2Zn_{20}$
Yb Wyckoff site	8*a*	8*a*	8*a*
Zn1 Wyckoff site	16*c*	16*c*	16*c*
Zn2 Wyckoff site	96*g*	96*g*	96*g*
Yb-Zn1 (Å)	3.0299(1)	3.0633(1)	3.0662(1)
Yb-Zn2 (Å)	3.0873(4)	3.0994(3)	3.0928(4)
Zn1-Zn2 (Å)	2.9859(3)	3.0075(3)	3.0059(4)
Zn2-Zn2 (Å)	2.6010(4)/ 2.6594(5)	2.6092(4)/ 2.6714(5)	2.6049(6)/ 2.6646(7)
Cage dimension (Å)	5.9113(4)	5.9549(4)	5.9515(5)
U_{iso} of Yb (Å)	0.00781(8)	0.00688(9)	0.00881(10)
θ_D (K)	239(265)	228(250)	224(240)
v (m/s)	3919	3826	3813
A (10^{-42} s^3)	8.8	12.4	17.5
B (10^{-18} s·K^{-1})	2.6	0.7	1.8
C (10^{33} s^{-3})	7.2	17.6	16
ω_0 (THz)	1.5	1.9	2.4
θ_E (K)	72(76)	91(95)	115(110)

of 30 to 60 microhm·cm for 12 K ≤ T ≤ 50 K. The Seebeck coefficient S exhibits a peak that is maximized for TM = Ir near 30 K at an enhanced value of −65 μV/K. ZT is calculated from these quantities and is found to be large, considering that it is a low-temperature value, especially for $YbIr_2Zn_{20}$ with a value of $ZT = 0.07$ at T = 35 K. This ZT value is nearly an order of magnitude larger than that of many competitive and well-known thermoelectric materials for cooling applications, particularly $Bi_{2-x}Sb_xTe_3$ (ZT ~ 0.008 at 35 K) and chemical analogs like $CsBi_4Te_6$ (ZT ~ 0.01 at 35 K) (*23*). From this, we propose that $YbTM_2Zn_{20}$ and the wider family of chemical analogs offer a long-desired stage upon which to develop a new generation of thermoelectric materials for low-temperature applications, e.g., for use in satellites or spacecraft and cryogenic cooling at temperatures below liquid nitrogen.

RESULTS

Single-crystal XRD

$YbTM_2Zn_{20}$ (TM = Co, Rh, Ir) crystallizes in space group Fd-$3m$ (#227) with Z = 8. Using the molten metal flux growth technique (*17–19*), we have obtained large single crystals of $YbTM_2Zn_{20}$ (several millimeters in size). For example, Fig. 1A shows the as-synthesized $YbCo_2Zn_{20}$, with the triangle face corresponding to the (111) crystallographic plane, indicating a [111] directional growth preference. Figure 1B shows the unit cell viewed along the [111] direction, suggesting a kagome lattice formed by the Yb and the transition metal atoms. Each Yb atom is surrounded by 16 Zn atoms and each TM is surrounded by 12 Zn atoms, thus forming two types of polyhedrons, Frank-Kasper polyhedron and icosahedron, respectively (Fig. 1C). The coordination between the Yb atoms and the TM-Zn cages is shown in Fig. 1 (D and E), where it is seen that there is no direct bonding between any Yb and TM atoms. For the Frank-Kasper polyhedron (Fig. 1F), the framework is formed by the 4 nearest neighbors (16*c*) and the 12 next nearest neighbors (96*g*) of the Zn atoms with Yb at the center. For this cluster, we define the cage dimension as the longest distance between the Zn atoms in the cage framework and list the diameters of the Frank-Kasper polyhedra in Table 1 (all are between 5.91 and 5.96 Å). The cage dimension changes slightly with the TM atoms, and the largest value was observed in $YbRh_2Zn_{20}$, presumably because of the larger covalent radius of Rh as compared to Co and Ir. Overall, the cage dimensions of $YbTM_2Zn_{20}$ have values that are comparable to those of the Yb-filled skutterudite $Yb_{0.1}CoSb_3$ and the skutterudite derivative $Yb_{0.14}Co_4Ge_6Se_6$, where the Yb ions exhibit "rattling" behavior (*24–26*), suggesting that similar behavior might be expected here. Although the atomic displacement parameters are relatively small (~0.01 Å) for the Yb ions, evidence for soft lattice phonon modes are observed from both the temperature-dependent κ_L and the heat capacity (C_p), which will be discussed in the light of understanding the phonon transport in these materials.

Thermoelectric property measurements

Temperature-dependent Seebeck coefficient (S) measurements (gradient sweep method), four-probe resistivity (ρ) measurements, and steady-state thermal conductivity (κ) measurements from 12 to 300 K were performed for single crystals of $YbTM_2Zn_{20}$ to characterize both PF and ZT. The single crystals were carefully aligned before mounting so that both the thermal gradient and the electrical current were along the [100] crystallographic direction. Figure 2 shows $S(T)$, where the low T values are large and negative. With increasing T, there are breaks in slope near 50 K for TM = Co and Rh, and a well-defined peak near 35 K for TM = Ir, consistent with the earlier reported Kondo lattice behavior (*6–9*). Above the peak temperature, the absolute value of S decreases with increasing temperature, eventually changing sign from negative to positive at 185 and 240 K for $YbCo_2Zn_{20}$ and $YbRh_2Zn_{20}$, respectively, indicating that there is a competition between electrons and hole regarding the dominant charge carrier type. This is consistent with results from band structure calculations, which show both electron and hole pockets near the Fermi level (*27*). We also note that the S value of $YbIr_2Zn_{20}$ remains negative up to 300 K but is estimated to have a crossover to positive values near 370 K. The inset of Fig. 2 shows ρ(T) for all three specimens. Similar behavior is seen between them, where ρ decreases with increasing temperature for 12 < T < 40 K and then increases, as expected from metallic transport. This is in agreement with earlier measurements, where the initial decrease seen here is the high temperature tail of a Kondo coherence peak that is centered at <10, 30, and 20 K for TM = Co, Rh, and Ir, respectively (*15–20*). Note that the varying values of the coherence temperature are due to the different hybridization strengths between the three compounds (*20*). The combination of enhanced S values and the relatively low ρ at low T results in large peak values in the power factor ($PF = S^2/\rho$) of 7, 35, and 74 μW/cm-K^2 for $YbCo_2Zn_{20}$, $YbRh_2Zn_{20}$, and $YbIr_2Zn_{20}$, respectively.

Because both electrical transport and thermal transport contribute to the efficiency of thermoelectricity, it is important to quantify the thermal properties of these compounds. To do this and to better understand the impact of the soft lattice phonon modes on the thermal

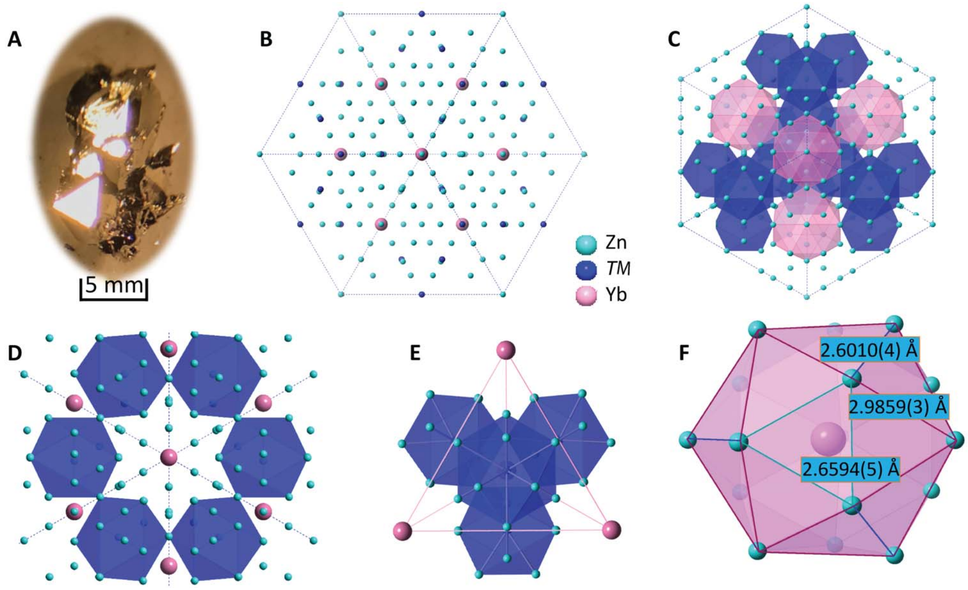

Fig. 1. Crystal structure and partial structures of YbTM_2Zn_{20}. (**A**) Single crystals of $YbCo_2Zn_{20}$ synthesized by flux growth method. (**B**) [111] directional view of the unit cell of YbTM_2Zn_{20}, suggesting kagome lattice formed by Yb and *TM* atoms. (**C**) Polyhedron representation of the unit cell. The coordination between Yb atoms and the *TM* cages with (**D**) Yb as the center and (**E**) *TM* cage as the center. (**F**) Frank-Kasper polyhedron formed by Yb and Zn atoms.

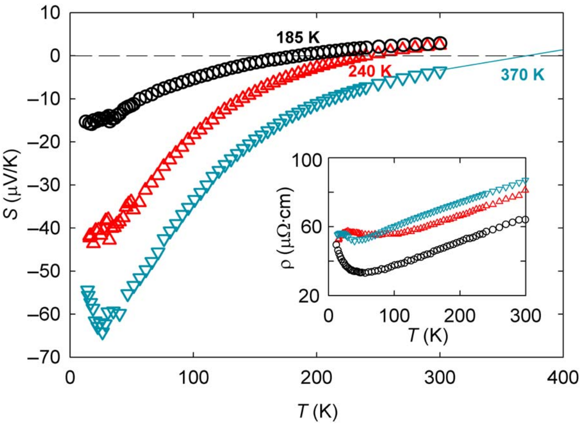

Fig. 2. Temperature-dependent Seebeck coefficient of $YbCo_2Zn_{20}$ (circle), $YbRh_2Zn_{20}$ (up-triangle), and $YbIr_2Zn_{20}$ (down-triangle). The dashed line indicates $S = 0$, and the solid line is an extrapolation of the S of $YbIr_2Zn_{20}$ at higher temperature. Inset: Temperature-dependent electrical resistivity of $YbCo_2Zn_{20}$ (circle), $YbRh_2Zn_{20}$ (up-triangle), and $YbIr_2Zn_{20}$ (down-triangle).

transport in these materials, we measured C_p (Fig. 3) and κ (Fig. 4) and estimated the Debye temperature (θ_D), the Einstein temperature (θ_E), and different phonon scattering parameters that represent the importance of different phonon scattering mechanisms. We first estimate θ_D, from the T^3 dependence of C_p, to be 239, 228, and 224 K for $YbCo_2Zn_{20}$, $YbRh_2Zn_{20}$, and $YbIr_2Zn_{20}$, respectively (straight line fit in Fig. 3 insets). A more detailed fit that incorporates both the Debye and Einstein models is also shown in Fig. 3 and yields similar values (see Table 1) (*28*). We note that C_p features a large electronic Sommerfeld coefficient at low temperature (insets of Fig. 3), just like what has been reported in earlier study, which suggests heavy-fermion behavior (*7–9*, *18–20*). This result also corroborates with the large effective mass obtained from the dHvA experiment (*14*).

Figure 4A shows κ from 12 to 300 K. Because of the large conventional unit cell (184 atoms per unit cell), the overall κ is relatively low. Applying the Wiedemann-Franz law where $\kappa_E = L_0\sigma T$ (L_0 is the Lorentz number), we obtain κ_L as a function of temperature from $\kappa - \kappa_E$ (Fig. 4B). Because of the low ρ values of YbTM_2Zn_{20}, κ is dominated by κ_E throughout the entire measured temperature range. The overall lower ρ of $YbCo_2Zn_{20}$, compared with that of the other two systems, contributes to higher κ_E and therefore to higher κ. After subtracting κ_E, κ_L for all three systems is quite similar, as expected for compounds that share the same structure. To estimate the corresponding phonon scattering parameters, we used the Debye approximation to fit κ_L (solid lines in Fig. 5B) using the expression (*29*)

$$\kappa_L = \frac{k_B}{2\pi^2\upsilon}\left(\frac{k_B T}{\upsilon}\right)^3 \int_0^{\theta_D/T} \frac{x^4 e^x}{\tau_C^{-1}(e^x - 1)^2}\,dx \qquad (1)$$

where $x = \hbar\omega/k_B T$ is dimensionless, υ is the speed of sound, and τ_C is the phonon scattering relaxation time. τ_C^{-1} can be further written as

$$\tau_C^{-1} = \frac{\upsilon}{L} + A\omega^4 + B\omega^2 T \exp\left(-\frac{\theta_D}{3T}\right) + \frac{C\omega^2}{(\omega_0^2 - \omega^2)^2} \qquad (2)$$

where L is the grain size, ω is the phonon frequency, ω_0 is the resonance frequency, and the coefficients A, B, and C are fit parameters. The terms in Eq. 2 represent grain boundary phonon scattering, point defect phonon scattering, Umklapp scattering, and resonance scattering, respectively. In our fits, the υ values were calculated from the elastic constant reported in (*16*). The fit parameters were defined using a minimization of best sequence fit functions as compared to the experimental data and are listed in Table 1 together with the other related physical parameters. Excluding the transition elements, in each formula unit, the average mass of each atom is about 70 g/mol. As the transition element changes from Co to Rh and then Ir, the mass

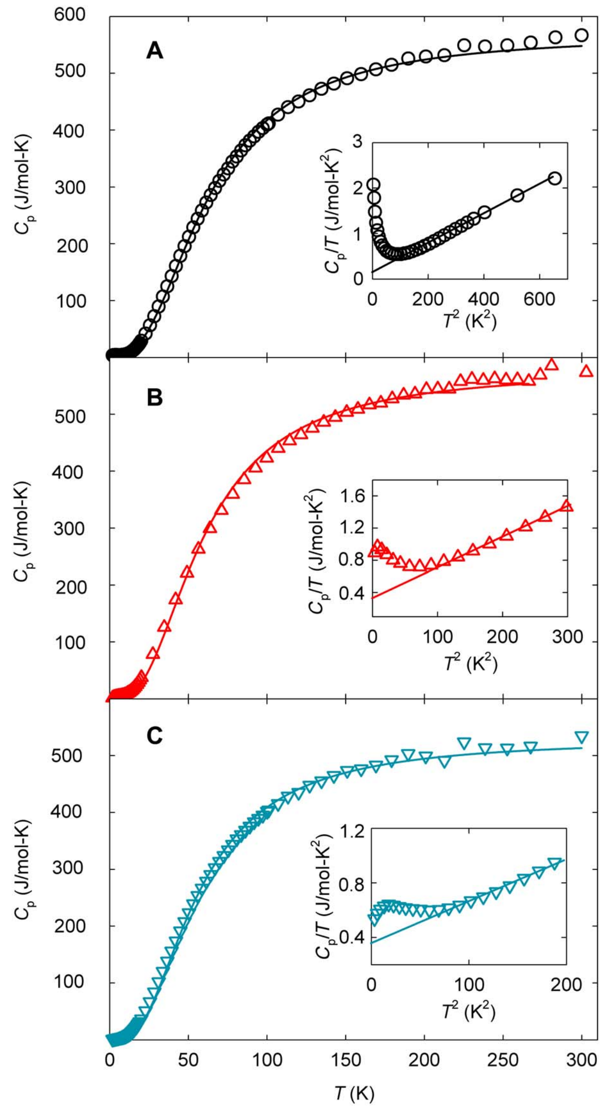

Fig. 3. Temperature-dependent heat capacity of Yb*TM*$_2$Zn$_{20}$. (**A**) YbCo$_2$Zn$_{20}$. (**B**) YbRh$_2$Zn$_{20}$. (**C**) YbIr$_2$Zn$_{20}$. Solid lines representing the fitting using a combined Debye-Einstein model: $C_P = C_D\left(\frac{T}{\theta_D}\right)^3\int_0^{\theta_D/T}\frac{x^4e^x}{(e^x-1)^2}dx + C_E\left(\frac{\theta_E}{T}\right)^2\frac{e^{\theta_E/T}}{(e^{\theta_E/T}-1)^2}$, where C_D and C_E are constants containing numbers of oscillators and degrees of freedom, respectively (*28*). The insets show C_p/T versus T^2 data at low temperatures, with the solid lines representing the $C_p/T = \gamma + \beta T^2$ relation.

difference between *TM* and the average atomic mass of the unit cell increases. This creates enhanced mass fluctuation scattering between *TM* and the rest of the atoms in the unit cell, as indicated by the increased point defect phonon scattering parameter *A*. To quantitatively investigate the effect of the transition metals on *B*, information about the Grüneisen parameters would be required, so this analysis is not presented. The constant ω_0 represents the rattling frequency of Yb atoms due to the dynamic disorder resonance, and from our fits, we obtain values of $\omega_0 \sim 2$ THz for all three specimens. This is as expected, because all three specimens have a similar cage size. We note that the ω_0 values of Yb*TM*$_2$Zn$_{20}$ are similar to those of Yb$_{0.19}$Co$_4$Sb$_{12-x}$Sn$_x$ (x = 0, 0.05, and 0.2), likely due to size similarity of the cages (*13*). On the basis of ω_0, we estimate Einstein temperatures ($\theta_E = h\omega_0/k_B$) to be 72, 91, and 115 K for YbCo$_2$Zn$_{20}$, YbRh$_2$Zn$_{20}$, and YbIr$_2$Zn$_{20}$, respectively. These values also agree quite well with the fitting results from C_p by applying a combined Debye-Einstein model (Table 1). Thus, the κ analysis shows that the cage-like structure, coupled with the soft lattice phonon modes, results in small κ_L values. This directly contributes to the overall low κ, which is essential for good thermoelectric materials.

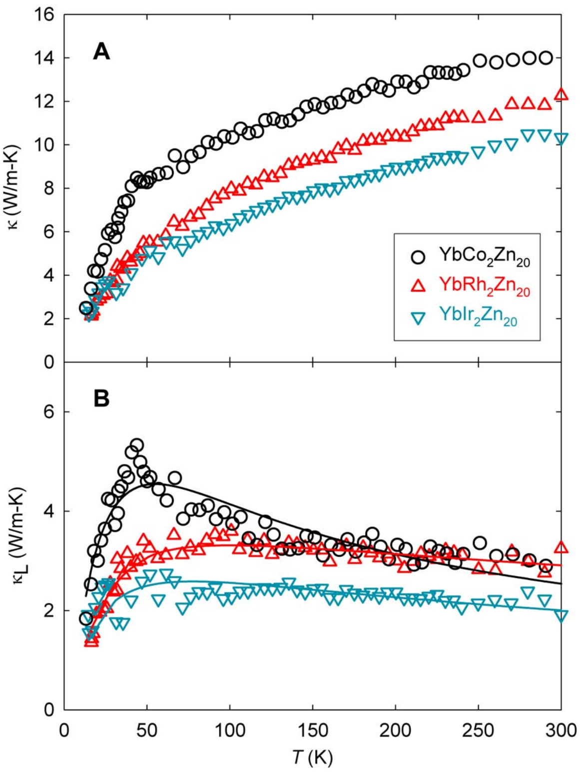

Fig. 4. Temperature-dependent thermal conductivity of Yb*TM*$_2$Zn$_{20}$. Temperature-dependent thermal conductivity (**A**) and lattice thermal conductivity (**B**) for YbCo$_2$Zn$_{20}$ (circle), YbRh$_2$Zn$_{20}$ (up-triangle), and YbIr$_2$Zn$_{20}$ (down-triangle). The solid lines are fits based on Eqs. 1 and 2 described in the text.

DISCUSSION

The large *PF* values of Yb*TM*$_2$Zn$_{20}$ compounds (Fig. 5A) and the small κ values result in remarkably large *ZT* values for all three compounds and across broad *T* ranges, with a maximum near *ZT* = 0.07 at 35 K for YbIr$_2$Zn$_{20}$ (Fig. 5B). To our knowledge, this is only second to Bi$_{1-x}$Sb$_x$ at this temperature (*ZT* = 0.15) (*30*). For comparison, the insets of Fig. 5 (A and B) show *PF* and *ZT* at 35 K for several well-known thermoelectric materials: FeSb$_2$ (*31*), Bi$_{0.5}$Sb$_{1.5}$Te$_3$ (thermoelectric material from Marlow industry), Bi$_2$Te$_3$ (thermoelectric material standard from the National Institute of Science and Technology), CsBi$_4$Te$_6$ (*23*), and YbAl$_3$ (*32*). The *ZT* value of YbIr$_2$Zn$_{20}$ is about an order of magnitude higher than these materials. Although YbAl$_3$ has large *PF* at low temperatures (*PF* = 200 at 35 K), due to the relatively large κ values the *ZT* value of YbAl$_3$ peaks with 0.04 at 100 K (*ZT* = 0.017 at 35 K) (*32*). We note that not many materials have been investigated with a focus on the thermoelectric performance at low temperatures. Considering the bulk thermodynamic and electrical transport measurements, we classify these compounds as phonon-glass, electron-crystal materials. We understand this behavior as resulting from (i) the Kondo coherent *f*-electron lattice (*7–9*, *18–20*) that leads

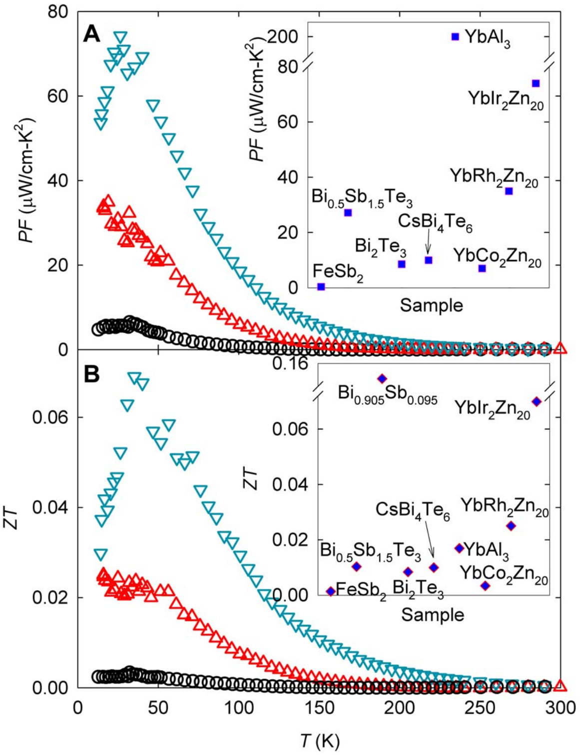

Fig. 5. Temperature-dependent power factor and thermoelectric figure of merit of YbTM_2Zn$_{20}$. Temperature-dependent (**A**) *PF* and (**B**) *ZT* of YbCo$_2$Zn$_{20}$ (circle), YbRh$_2$Zn$_{20}$ (up-triangle), and YbIr$_2$Zn$_{20}$ (down-triangle). The insets in (A) and (B) are the *PF* and *ZT* values of several well-known thermoelectric materials at 35 K plotted together with parent compounds.

to both low ρ and a peak in *S*, which combine to yield an enhanced *PF* at low temperatures, and (ii) the low κ that results from the soft lattice modes. This finding opens the door to investigating 1-2-20 family of materials as the next-generation materials for low-temperature thermoelectric applications.

There are several strategies to further increase *ZT* in the temperature region where the power factor has its peak value. From the "phonon-glass" point of view, κ will need to be further reduced. This can be achieved by modifying the soft lattice modes. In similar skutterudite systems, κ_L is greatly reduced by using multiple rare earth atoms to fill the cages. This introduces multispectral rattling frequencies that resonate with a broad spectrum of phonon frequencies (*33*). In addition, the maximum mass fluctuation phonon scattering was observed at a 50% filling fraction of the cages in rare earth–filled skutterudites (*34*). These approaches can be directly adapted to the 1-2-20 compounds as effective ways to substantially reduce κ without disturbing the electrical transport. Moreover, because grain boundary phonon scattering dominates κ_L at the very lowest temperatures, reducing the size of the single domains could provide an alternative way to reduce κ_L, thereby improving the *ZT* values, due to the effect of significant interface scatterings at the grain boundaries (*35*, *36*).

Alternatively, the electrical properties could be tuned by composition modifications to enhance the *PF* of these materials. Because of the Kondo lattice hybridization, the ρ(*T*) value of the 1-2-20 materials decreases with decreasing temperature below the coherence temperatures (*18*–*20*). The sharp change of the density of states near the Fermi level, contributed by the elements with unstable valences, results in a large *S* (*7*–*9*). By substituting Yb with other rare earth elements or actinides that feature different Kondo energy scales (e.g., Ce, Tm, Eu, or U), changes in both the peak values of *PF* and the temperature region for *PF* to peak can be expected. Such tunability can be investigated to alter the temperature region in which these 1-2-20 materials can be applied for efficient thermoelectric energy conversion applications. Moreover, because both n- and p-type thermoelectric materials are needed to construct thermoelectric modules, replacing Yb with Ce could be of great interest as Ce and Yb are electron/hole analogs.

In summary, we have synthesized high-purity single crystalline YbTM_2Zn$_{20}$ (TM = Co, Rh, Ir) using the molten flux growth method. In addition to the large conventional unit cell, we observed soft lattice phonon modes that produce a further reduced κ_L. The Kondo lattice hybridization in these heavy-fermion materials also results in low ρ and enhanced *S* at low temperatures. This combination of phenomena allows these materials to achieve enhanced thermoelectric properties. In particular, we obtain a *ZT* value of 0.07 at 35 K for YbIr$_2$Zn$_{20}$ and a corresponding large *PF*. Having addressed that, in order for these materials to be interesting for device applications, the maximum cooling power will need to be improved. We also propose several different approaches to tune and further improve the thermoelectric properties of the 1-2-20 materials. Our results provide new momentum to the concept that heavy-fermion systems with cage-like structures are potentially promising for thermoelectric applications.

MATERIALS AND METHODS

Sample synthesis

The title compounds were synthesized by molten flux growth method. Yb chunks (99.9%, Ames Labs), Co ingots (99.99%, Alfa Aesar), Rh ingots (99.99%, Alfa Aesar), Ir ingots (99.99%, Alfa Aesar), and Zn shot (99.999%, Alfa Aesar) in an atomic ratio of Yb:*TM*:Zn (*TM* = Co, Rh, Ir) = 1:2:60 were loaded into 2-ml alumina crucibles and sealed under vacuum in quartz tubes. The quartz tubes were then heated to 1050°C at a rate of 50°C/hour, held at 1050°C for 24 hours, and then cooled to 700°C at a rate of 4°C/hour. At this temperature, the remaining flux was separated from the crystals by centrifugation. Multimillimeter-size single crystals were obtained.

Single-crystal XRD

YbTM_2Zn$_{20}$ single-crystals were characterized structurally by single-crystal XRD using an Oxford-Diffraction Xcalibur2 CCD system with graphite monochromated Mo *K*α radiation. Data were collected using ω scans with 1° frame widths to a resolution of 0.4 Å, equivalent to 2θ ≈ 125°. Reflections were recorded, indexed, and corrected for absorption using the Oxford-Diffraction CRYSALISPRO software (*37*), and subsequent structure determination and refinement were carried out using the single-crystal x-ray structure refinement and analysis software package CRYSTALS (*38*), with SUPERFLIP (*39*) phasing algorithm on F^2. The data quality allowed an unconstrained full matrix refinement against F^2 with anisotropic thermal displacement parameters for all atoms. The crystallographic information files have been deposited with the Inorganic Crystal Structure Database (ICSD CSD-434009, CSD-434010, and CSD-434011 for YbCo$_2$Zn$_{20}$, YbRh$_2$Zn$_{20}$, and YbIr$_2$Zn$_{20}$, respectively). Electron-dispersive spectroscopy analyses corroborated the stoichiometries obtained from the refinement results.

Transport property measurements

The single crystals of YbTM_2Zn_{20} were aligned on an Enraf-Nonius CAD-4 diffractometer along their [100] axis before being cut into rectangular slabs of 2 mm by 1 mm by 0.5 mm dimensions for temperature-dependent four-probe ρ, *S* (gradient sweep method), and steady-state κ measurements in the temperature range from 12 to 300 K. The crystals were mounted such that the current and thermal gradient were along the [100] direction. All the surfaces were polished using 3-μm grid diamond polishing paper to reduce surface radiation losses during the measurements. The measurements were carried out in a custom radiation-shielded vacuum probe with uncertainties of 4, 6, and 8% for ρ, *S*, and κ measurements, respectively (*40*). Electrical contacts to the specimens were made using silver epoxy, and thermal contacts were made using Stycast epoxy.

REFERENCES AND NOTES

1. G. A. Slack, in *CRC Handbook of Thermoelectrics*, D. M. Rowe, Ed. (CRC, 1995), 407 pp.
2. B. C. Sales, D. Mandrus, R. K. Williams, Filled skutterudite antimonides: A new class of thermoelectric materials. *Science* **272**, 1325–1328 (1996).
3. G. S. Nolas, D. T. Morelli, T. M. Tritt, SKUTTERUDITES: A phonon-glass-electron crystal approach to advanced thermoelectric energy conversion applications. *Annu. Rev. Mater. Res.* **29**, 89–116 (1999).
4. B. C. Sales, Novel thermoelectric materials. *Curr. Opin. Solid State Mater. Sci.* **2**, 284–289 (1997).
5. G. D. Mahan, J. O. Sofo, The best thermoelectric. *Proc. Natl. Acad. Sci. U.S.A.* **93**, 7436–7439 (1996).
6. N. R. Dilley, E. D. Bauer, M. B. Maple, S. Dordevic, D. N. Basov, F. Freibert, T. W. Darling, A. Migliori, B. C. Chakoumakos, B. C. Sales, Thermoelectric and optical properties of the filled skutterudite $YbFe_4Sb_{12}$. *Phys. Rev. B* **61**, 4608–4614 (2000).
7. P. Swatek, D. Kaczorowski, Intermediate valence behavior in the novel cage compound $CeIr_2Zn_{20}$. *J. Phys. Condens. Matter* **25**, 055602 (2013).
8. S. Paschen, A. Bentien, S. Budnyk, A. M. Strydom, Y. Grin, F. Steglich, Strongly correlated cage compounds for thermoelectric applications?, in *Proceedings of the 25th International Conferences on Thermoelectrics* (IEEE, 2006), pp. 168–171.
9. R. J. Gambino, W. D. Grobman, A. M. Toxen, Anomalously large thermoelectric cooling figure of merit in the Kondo systems $CePd_3$ and $CeIn_3$. *Appl. Phys. Lett.* **22**, 506–507 (1973).
10. R. E. Baumbach, M. B. Maple, in *Encyclopedia of Materials: Science and Technology*, K. H. J. Buschow, R. W. Cahn, M. C. Flemings, B. Ilschner, E. J. Kramer, S. Mahajan, P. Veyssière, Eds. (Elsevier Ltd., 2010), chap. 11, pp. 1–6.
11. T. Nasch, W. Jeitschko, U. C. Rodewald, Ternary rare earth transition metal zinc compounds RT_2Zn_{20} with T = Fe, Ru, Co, Rh, and Ni. *Z. Naturforsch. B Chem. Sci.* **52**, 1023–1030 (1997).
12. Y. Dong, K. Wei, G. S. Nolas, Transport properties of partially filled skutterudite derivatives $Ce_{0.13}Co_4Ge_6Se_6$ and $Yb_{0.14}Co_4Ge_6Se_6$. *Phys. Rev. B* **87**, 195203 (2013).
13. J. Yang, D. T. Morelli, G. P. Meisner, W. Chen, J. S. Dyck, C. Uher, Effect of Sn substituting for Sb on the low-temperature transport properties of ytterbium-filled skutterudites. *Phys. Rev. B* **67**, 165207 (2003).
14. M. Ohya, M. Matsushita, S. Yoshiuchi, T. Takeuchi, F. Honda, R. Settai, T. Tanaka, Y. Kubo, Y. Ōnuki, Strong field quenching of the quasiparticle effective mass in heavy fermion compound $YbCo_2Zn_{20}$. *J. Phys. Soc. Jpn.* **79**, 083601 (2010).
15. Y. Hirose, M. Toda, S. Yoshiuchi, S. Yasui, K. Sugiyama, F. Honda, M. Hagiwara, K. Kindo, R. Settai, Y. Ōnuki, Metamagnetic transition in heavy fermion compounds YbT_2Zn_{20} (T: Co, Rh, Ir). *J. Phys. Conf. Ser.* **273**, 012003 (2011).
16. Y. Nakanishi, T. Kamiyama, K. Ito, M. Nakamura, Y. Saiga, M. Kosaka, Y. Uwatoko, M. Yoshizawa, Ultrasonic investigation close to quantum critical point in $YbTr_2Zn_{20}$ (Tr: Co, Rh, and Ir). *J. Phys. Conf. Ser.* **200**, 012142 (2010).
17. S. Jia, N. Ni, S. L. Bud'ko, P. C. Canfield, Magnetic properties of RFe_2Zn_{20} and RCo_2Zn_{20} (R=Y, Nd, Sm, Gd–Lu). *Phys. Rev. B* **80**, 104403 (2009).
18. F. Honda, T. Takeuchi, S. Yasui, Y. Taga, S. Yoshiuchi, Y. Hirose, Y. Tomooka, K. Sugiyam, M. Hagiwara, K. Kindo, R. Settai, Y. Ōnuki, Metamagnetic behavior and effect of pressure on the electronic state in heavy-fermion compound $YbRh_2Zn_{20}$. *J. Phys. Soc. Jpn.* **82**, 084705 (2013).
19. Y. Ōnuki, S. Yasui, M. Matsushita, S. Yoshiuchi, M. Ohya, Y. Hirose, N. D. Dung, F. Honda, T. Takeuchi, R. Settai, K. Sugiyama, E. Yamamoto, T. D. Matsuda, Y. Haga, T. Tanaka, Y. Kubo, H. Harima, Characteristic heavy fermion properties in $YbCu_2Si_2$ and YbT_2Zn_{20} (T: Co, Rh, Ir). *J. Phys. Soc. Jpn.* **80**, SA003 (2011).
20. M. S. Torikachvili, S. Jia, E. D. Mun, S. T. Hannahs, R. C. Black, W. K. Neils, D. Martien, S. L. Bud'ko, P. C. Canfield, Six closely related YbT_2Zn_{20} (T = Fe, Co, Ru, Rh, Os, Ir) heavy fermion compounds with large local moment degeneracy. *Proc. Natl. Acad. Sci. U.S.A.* **104**, 9960–9963 (2007).
21. S. R. Brown, S. M. Kauzlarich, F. Gascoin, G. J. Snyder, $Yb_{14}MnSb_{11}$: New high efficiency thermoelectric material for power generation. *Chem. Mater.* **18**, 1873–1877 (2006).
22. A. Bentien, E. Nishibori, S. Paschen, B. B. Iversen, Crystal structures, atomic vibration, and disorder of the type-I thermoelectric clathrates $Ba_8Ga_{16}Si_{30}$, $Ba_8Ga_{16}Ge_{30}$,$Ba_8In_{16}Ge_{30}$, and $Sr_8Ga_{16}Ge_{30}$. *Phys. Rev. B* **71**, 144107 (2005).
23. D.-Y. Chung, T. P. Hogan, M. Rocci-Lane, P. Brazis, J. R. Ireland, C. R. Kannewurf, M. Bastea, C. Uher, M. G. Kanatzidis, A new thermoelectric material: $CsBi_4Te_6$. *J. Am. Chem. Soc.* **126**, 6414–6428 (2004).
24. D. J. Braun, W. Jeitschko, Preparation and structural investigations of antimonides with the $LaFe_4P_{12}$ structure. *J. Less Common Metals* **72**, 147–156 (1980).
25. G. A. Slack, V. G. Tsoukala, Some properties of semiconducting $IrSb_3$. *J. Appl. Phys.* **76**, 1665–1671 (1994).
26. D. Bérardan, E. Alleno, C. Godart, O. Rouleau, J. Rodriguez-Carvajal, Preparation and chemical properties of the skutterudites $(Ce–Yb)_yFe_{4-x}(Co/Ni)_xSb_{12}$. *Mater. Res. Bull.* **40**, 537–551 (2005).
27. T. Tanaka, Y. Kubo, Electronic structure of heavy-fermion systems YbT_2Zn_{20} (T = Fe, Co, Ru, Rh, Os, Ir). *J. Phys. Soc. Jpn.* **79**, 124710 (2010).
28. C. Kittel, *Introduction to Solid State Physics* (John Wiley & Sons Inc., ed. 7, 1996).
29. J. Callaway, Model for lattice thermal conductivity at low temperatures. *Phys. Rev.* **113**, 1046–1051 (1959).
30. B. Lenoir, M. Cassart, J.-P. Michenaud, H. Scherrer, S. Scherrer, Transport properties of Bi-rich Bi-Sb alloys. *J. Phys. Chem. Solids* **57**, 89–99 (1996).
31. K. Wei, J. Martin, G. S. Nolas, Synthesis, SPS processing and low temperature transport properties of polycrystalline $FeSb_2$ with nano-scale grains. *Mater. Lett.* **122**, 289–291 (2014).
32. D. M. Rowe, V. L. Kuznetsov, L. A. Kuznetsova, G. Min, Electrical and thermal transport properties of intermediate-valence $YbAl_3$. *J. Phys. D. Appl. Phys.* **35**, 2183–2186 (2002).
33. X. Shi, J. Yang, J. R. Salvador, M. Chi, J. Y. Cho, H. Wang, S. Bai, J. Yang, W. Zhang, L. Chen, Multiple-filled skutterudites: High thermoelectric figure of merit through separately optimizing electrical and thermal transports. *J. Am. Chem. Soc.* **133**, 7837–7846 (2011).
34. G. P. Meisner, D. T. Morelli, S. Hu, J. Yang, C. Uher, Structure and lattice thermal conductivity of fractionally filled skutterudites: Solid solutions of fully filled and unfilled end members. *Phys. Rev. Lett.* **80**, 3551–3554 (1998).
35. M. S. Dresselhaus, G. Chen, M. Y. Tang, R. G. Yang, H. Lee, D. Z. Wang, Z. F. Ren, J.-P. Fleurial, P. Gogna, New directions for low-dimensional thermoelectric materials. *Adv. Mater.* **19**, 1043–1053 (2007).
36. B. C. Sales, O. Delaire, M. A. McGuire, A. F. May, Thermoelectric properties of Co-, Ir-, and Os-doped FeSi alloys: Evidence for strong electron-phonon coupling. *Phys. Rev. B* **83**, 125209 (2011).
37. Agilent Technologies, *CRYSALISPRO, Version 1.171.37.33* (Agilent Technologies UK Ltd., 2014).
38. P. W. Betteridge, J. R. Carruthers, R. I. Cooper, K. Prout, D. J. Watkin, CRYSTALSversion 12: Software for guided crystal structure analysis. *J. Appl. Crystallogr.* **36**, 1487 (2003).
39. L. Palatinus, G. Chapuis, SUPERFLIP—A computer program for the solution of crystal structures by charge flipping in arbitrary dimensions. *J. Appl. Crystallogr.* **40**, 786–790 (2007).
40. J. Martin, G. S. Nolas, Apparatus for the measurement of electrical resistivity, Seebeck coefficient, and thermal conductivity of thermoelectric materials between 300 K and 12 K. *Rev. Sci. Instrum.* **87**, 015105 (2016).

Acknowledgments

Funding: This work was performed at the National High Magnetic Field Laboratory, which is supported by NSF Cooperative Agreement No. DMR-1644779 and the State of Florida. The synthesis of single crystals was supported by the Center for Actinide Science and Technology (CAST), an Energy Frontier Research Center funded by the U.S. Department of Energy, Office of Science, Basic Energy Sciences under award no. DESC0016568. K.W. acknowledges the support of the Jack E. Crow Postdoctoral Fellowship. J.N.N. and T.S. acknowledge support from the NSF under award NSF DMR-1606952. G.S.N. acknowledges support from the NSF (grant no. DMR-1748188). G.S.N. and D.H. also acknowledge support from the II-VI Foundation Block-Gift Program. **Author**

contributions: The crystals were grown by K.W. and characterized by J.N.N. K.W. performed the measurements with assistance from Y.L., K.-W.C., D.H., and D.E.G. Analyses of the results were done by K.W. and D.H. The manuscript was written by K.W. and R.E.B. with contributions from all authors. **Competing interests:** The authors declare that they have no competing interests. **Data and materials availability:** All data needed to evaluate the conclusions in the paper are present in the paper and/or the Supplementary Materials. Additional data related to this paper may be requested from the authors.

Submitted 14 January 2019
Accepted 23 April 2019
Published 31 May 2019
10.1126/sciadv.aaw6183

Citation: K. Wei, J. N. Neu, Y. Lai, K.-W. Chen, D. Hobbis, G. S. Nolas, D. E. Graf, T. Siegrist, R. E. Baumbach, Enhanced thermoelectric performance of heavy-fermion compounds YbTM_2Zn$_{20}$ (TM = Co, Rh, Ir) at low temperatures. *Sci. Adv.* **5**, eaaw6183 (2019).

Science Advances

Enhanced thermoelectric performance of heavy-fermion compounds YbTM_2Zn$_{20}$ (TM = Co, Rh, Ir) at low temperatures

Kaya Wei, Jennifer N. Neu, You Lai, Kuan-Wen Chen, Dean Hobbis, George S. Nolas, David E. Graf, Theo Siegrist and Ryan E. Baumbach

Sci Adv **5** (5), eaaw6183.
DOI: 10.1126/sciadv.aaw6183

Science Advances (ISSN 2375-2548) is published by the American Association for the Advancement of Science, 1200 New York Avenue NW, Washington, DC 20005. The title *Science Advances* is a registered trademark of AAAS.